Science Advances
AAAS

advances.sciencemag.org/cgi/content/full/4/10/eaat5847/DC1

Supplementary Materials for

Microphysiological 3D model of amyotrophic lateral sclerosis (ALS) from human iPS-derived muscle cells and optogenetic motor neurons

Tatsuya Osaki, Sebastien G. M. Uzel, Roger D. Kamm*

*Corresponding author. Email: rdkamm@mit.edu

Published 10 October 2018, *Sci. Adv.* **4**, eaat5847 (2018)
DOI: 10.1126/sciadv.aat5847

The PDF file includes:

Other Supplementary Material for this manuscript includes the following:

(available at advances.sciencemag.org/cgi/content/full/4/10/eaat5847/DC1)

Movie S3 (.mp4 format). Representative movie of muscle contraction after stimulation with glutamic acid on day 14.
Movie S4 (.mp4 format). Muscle contraction of the ALS motor unit after 1-Hz optical stimulation without drug.
Movie S5 (.mp4 format). Muscle contraction of the ALS motor unit after 1-Hz optical stimulation with rapamycin.
Movie S6 (.mp4 format). Muscle contraction of the ALS motor unit after 1-Hz optical stimulation with rapamycin and bosutinib.

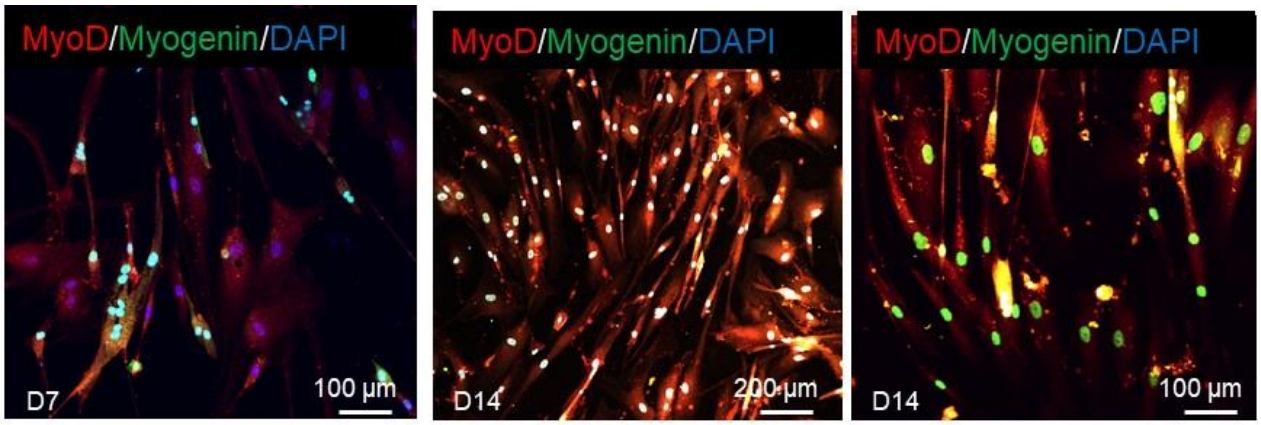

Fig. S1. Characterization and differentiation of iPS-derived skeletal myoblasts in a monolayer culture. Differentiation into a mature myotube was characterized in a petri dish by immunostaining of MyoD and myogenin. After D7 of differentiation, skeletal myoblasts partially expressed myogenin which is mature myocyte marker although almost all myoblasts expressed MyoD. After D14 of differentiation, myogenin expression can be seen in almost all myoblasts.

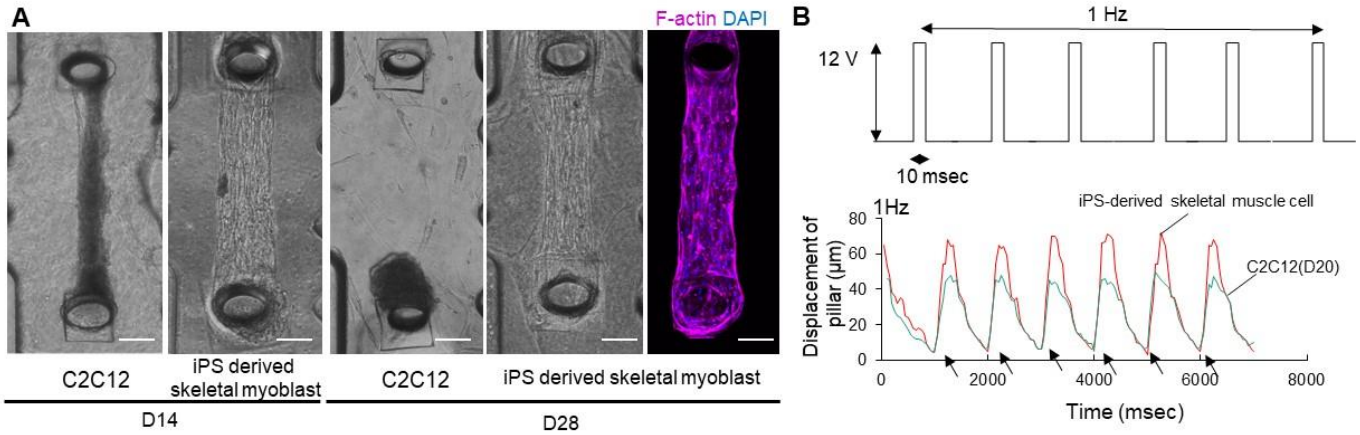

Fig. S2. Comparison between a mouse muscle fiber bundle of C2C12 and a human muscle fiber bundle of iPS-derived skeletal muscle cells. (A) Both mouse and human muscle fiber bundles were formed in the microfluidic device attaching the pillars on D14. However, C2C12 muscle fiber bundles break and collapse causing them to detach from the pillars, whereas human muscle fiber bundles maintain their structural integrity. (B) Pillar displacement by muscle contraction results when applying electrical stimulus. Displacement of iPS-skeletal muscle cells was higher than C2C12 on D20.

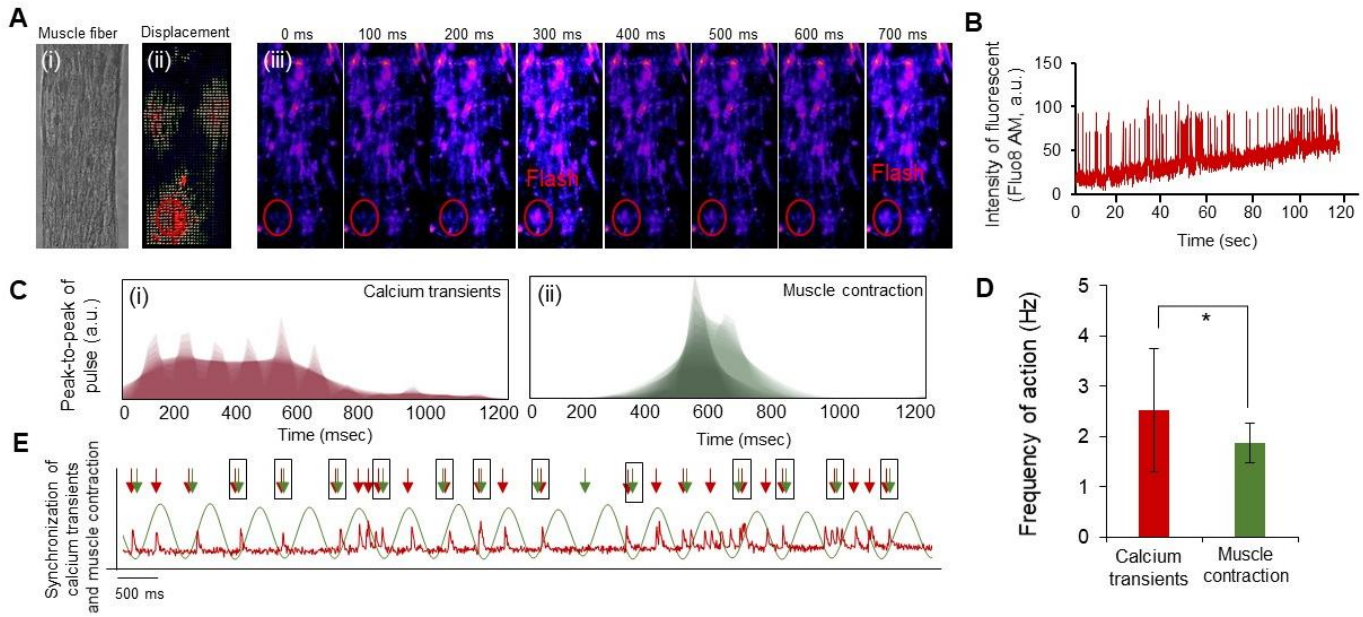

Fig. S3. Muscle contraction and synchronization by chemical stimulation. (A) Ca^{2+} imaging on muscle fiber bundle. (i) phase contrast imaging (ii) muscle force map (iii), neural firing on muscle fiber bundle every 100 ms. (B) Changes in the fluorescence intensity of the red circle in Figure 5A, indicating Ca^{2+} oscillation. (C) Histogram of peak-to-peak duration of calcium transients in the muscle fiber bundle and end feet of motor neurons and frequency of muscle contraction. (n = 7). (D) The difference of frequency between the calcium transients in the muscle fiber and muscle contraction (n = 60, 7 biological replicates). (E) Synchronization of calcium transients and muscle contraction. Black box indicates when calcium transients in the muscle fiber bundle coincide with muscle contraction. *, P<0.05, by Student's t test and one-way ANOVA. Error bars ± SD.

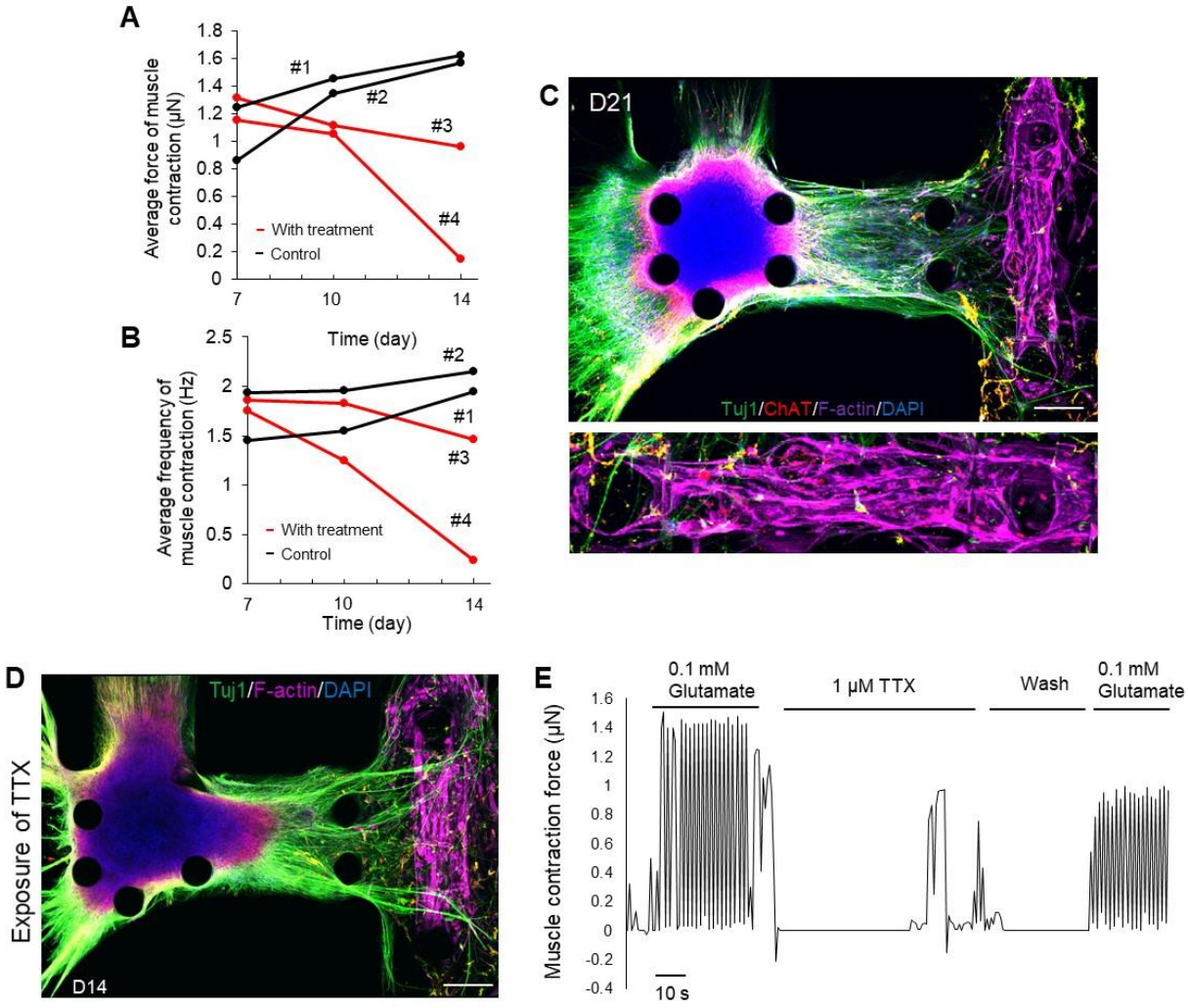

Fig. S4. Glutamic acid treatment and electrical stimulation and TTX treatment to the motor unit model. (A, B) Average force of muscle contraction and frequency after treatment with glutamic acid. (C) Muscle atrophy by continuous treatment of glutamic acid on D21. Representative images of human motor unit after TTX treatment. No significant difference can be seen in terms of morphology compared to before TTX treatment (1 μM). (E) TTX treatment completely prevented muscle contraction by preventing motor neural activity and connections. Then, after washing TTX, muscle contraction was recovered. Scale bar is 200 μm (D).

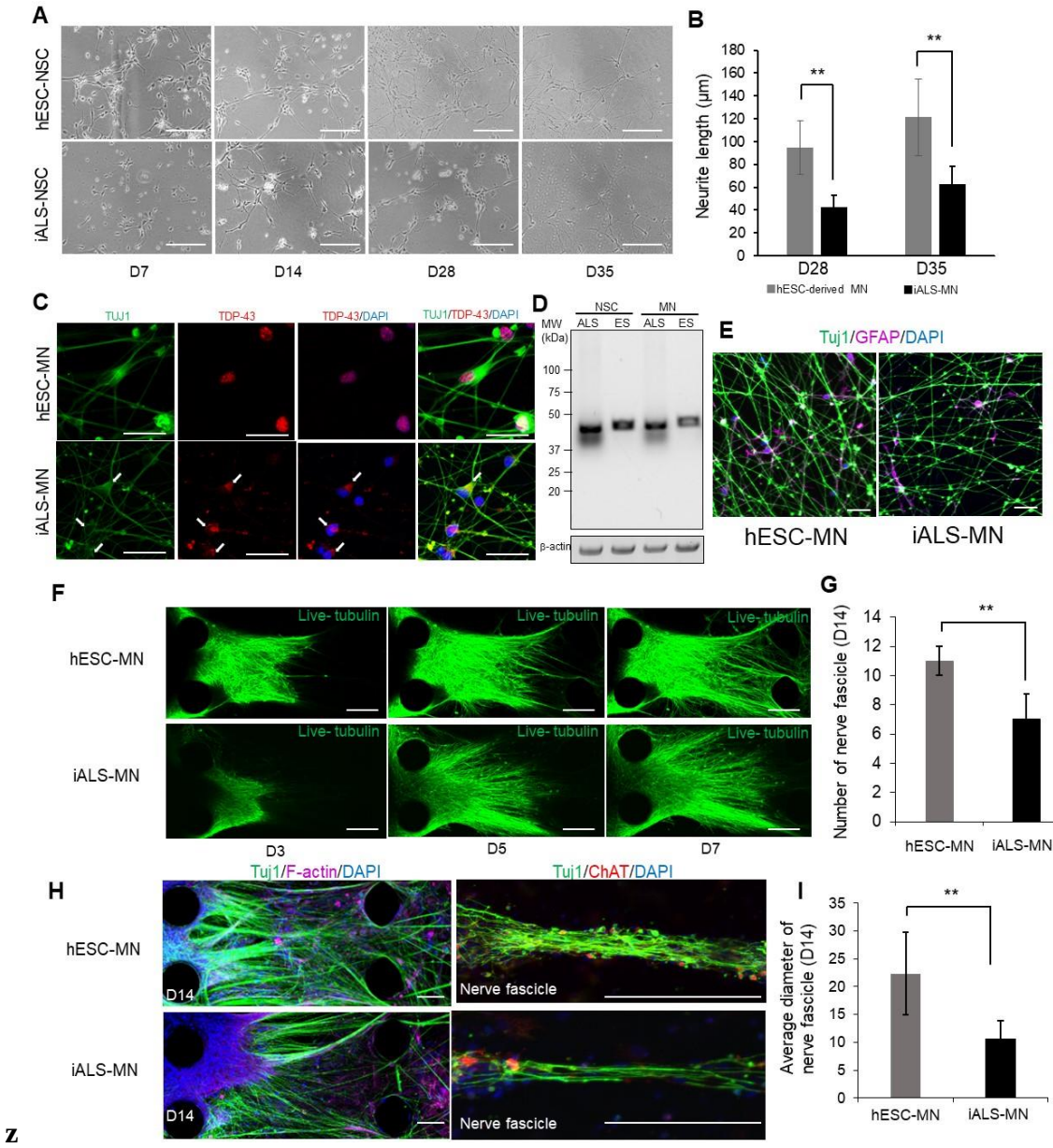

Fig. S5. Characterization of iPS-derived MN from a sporadic ALS donor. (A, B) Morphology of neural stem cells differentiating into MN from ALS-derived NSC and ES-derived NSC show significantly less elongation of neurites at D28 and D35 in 2D culture. (C) Deposition of TDP-43 aggregation at the cytoplasm of ALS-iPS derived MN. No aggregation can be seed in ES-derived MN. (D) Insoluble TDP-43 fractions from ALS and ES derived MN and NSC by western blotting. (E) Immunostaining of GFAP and Tuj1 showing neuron networks and astrocytes. (F) Speed of neurite elongation in microfluidic device after injecting pre-differentiated MN spheroids. Tubulin structure was live-stained in cells prior to injection to the micro devices, then observed at D3, D5, and D7. (G) The number of nerve fascicles of ALS-iPS MN is lower than ES-derived MN. (H) Magnified view of Tuj-1 staining showed significant differences in the thickness of nerve fascicles between the two motor unit models. (I) Average diameter of nerve fascicles at D14. (n = 4) **, $P<0.01$. Student t-test. Scale bars are 50 μm (C, E) and 100 μm (A, F, H).

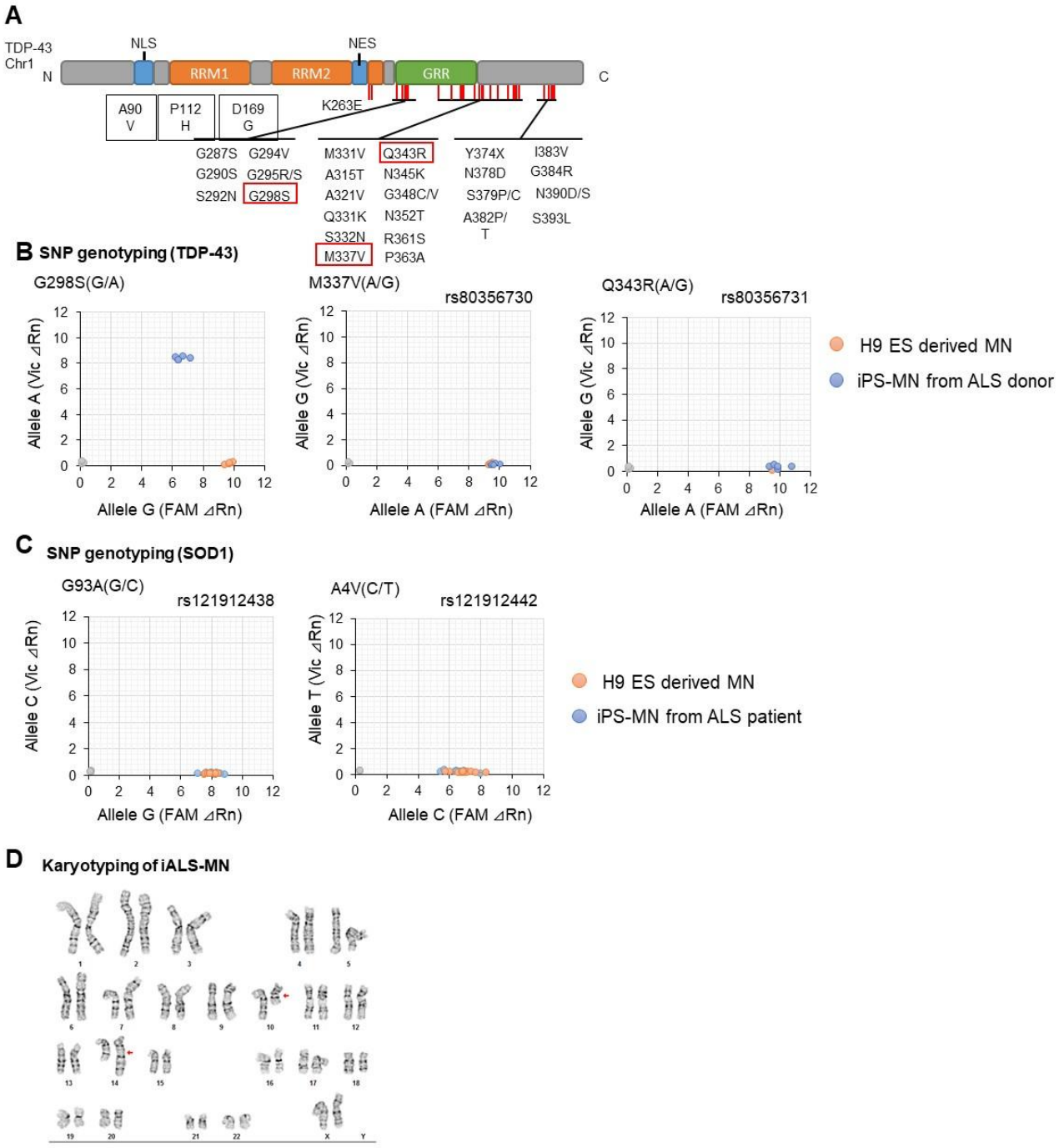

Fig. S6. Genotyping of ALS-iPS–derived MN and ES-derived MN. (A) The typical SNP mutation at TDP-43. (B) ALS iPS-derived MNs are heterozygous for G298S and homozygous for M337V and Q343R, whereas ES-derived MN has no mutation related to these three SNP mutations. (C) No SOD1 mutation of A4V and G93A in either type of MN cells. (D) G-band karyotyping analysis of parental ALS-iPSC.

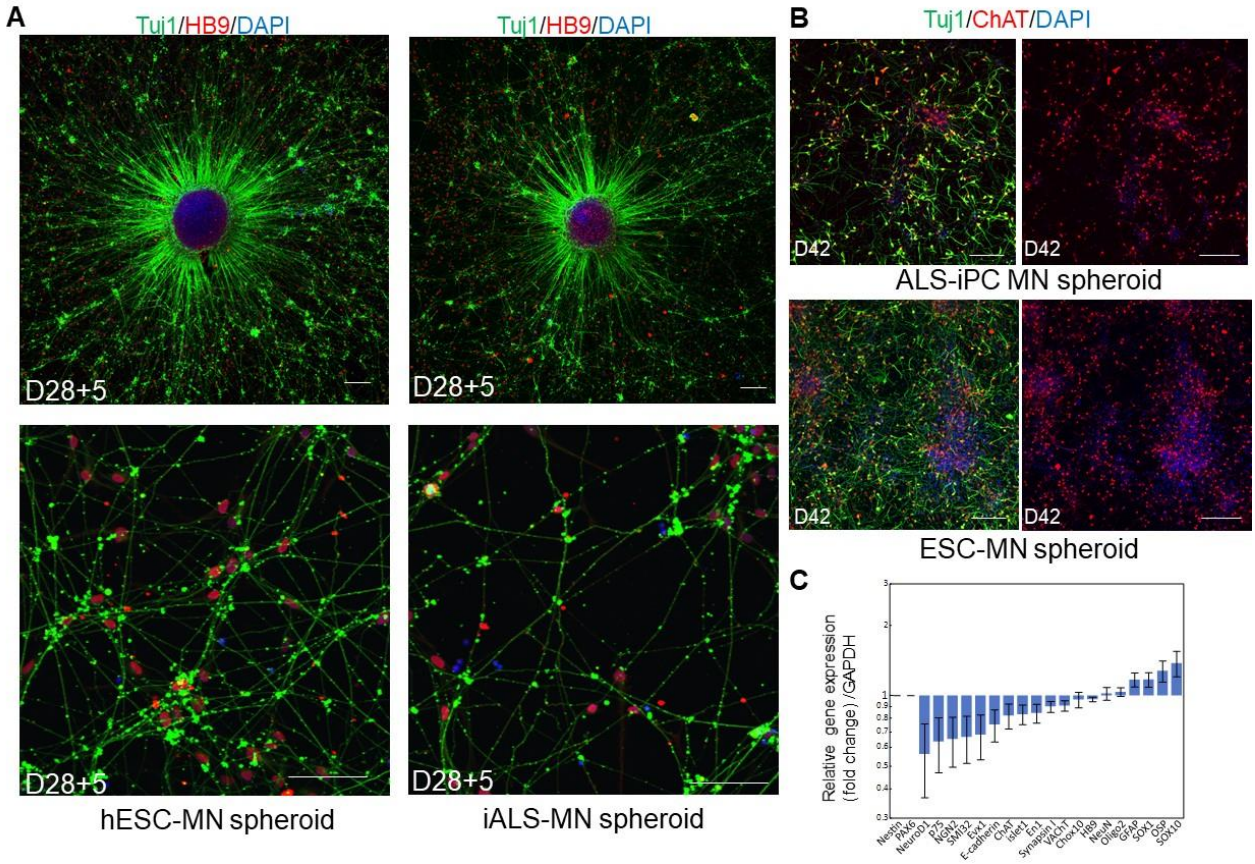

Fig. S7. Morphogenesis of MN spheroids derived from a patient with ALS in 2D culture. (A) Pre-differentiated (D28) MN spheroid was reseeded on PLO-laminin coated surface and cultured for an additional 5 days, then stained for Tuj1, HB9, and DAPI. The density of elongated neurites extending from the MN spheroid from ALS patient cells is significantly lower compared with the ESC-derived MN spheroid. The amount of HB9 expression is the same between the two models, consistent with the real-time PCR. (B) Immunostaining of ChAT in the two models. (C) The phenotypic difference of iALS-MN spheroids compared to ESC-MN spheroids after co-culture with muscle tissues in microfluidic devices. Scale bar is 100 μm.

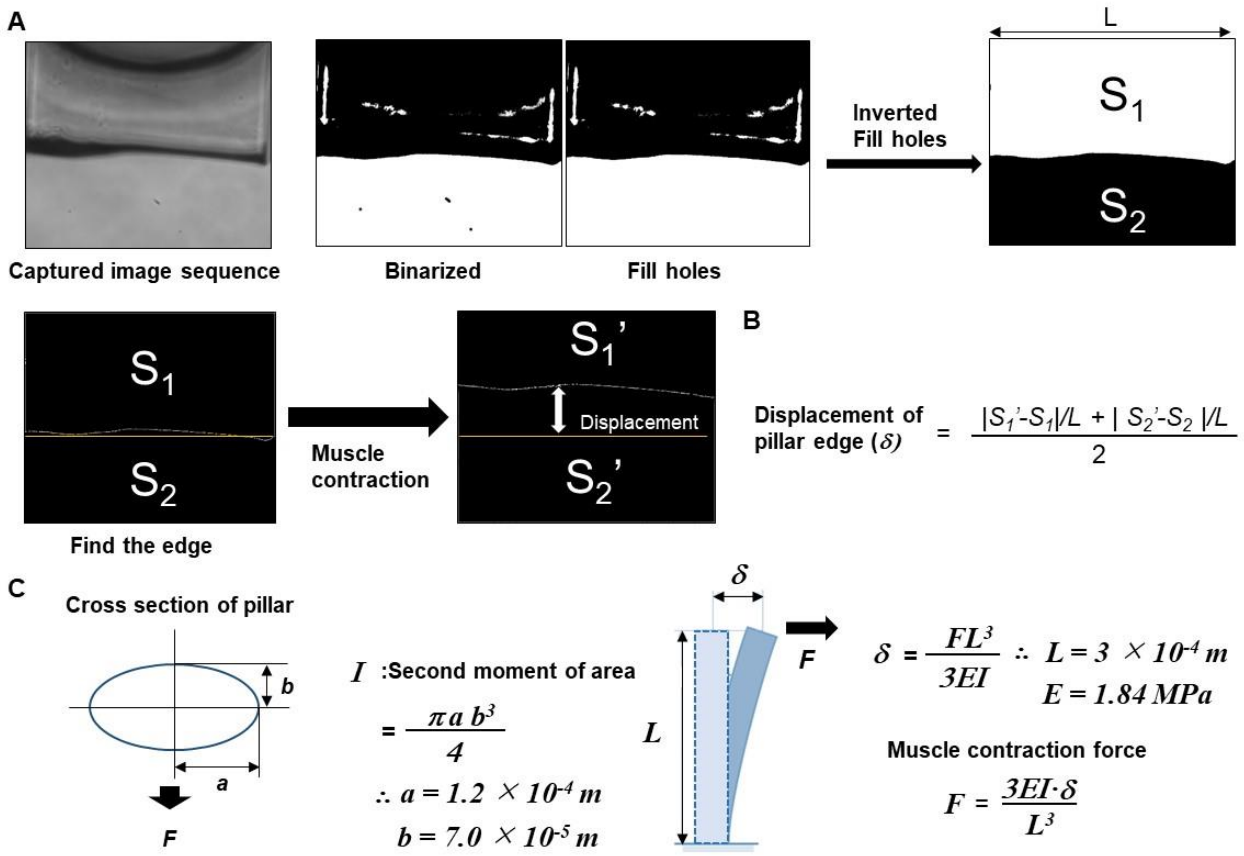

Fig. S8. Automated detection of pillar displacement, estimating muscle contraction. (A) Captured videos were analyzed using Python with OpenCV plugin. (B) Formula used to calculate displacement of the pillar edge. (C) Calculation of muscle contraction force from pillar displacement measurements.

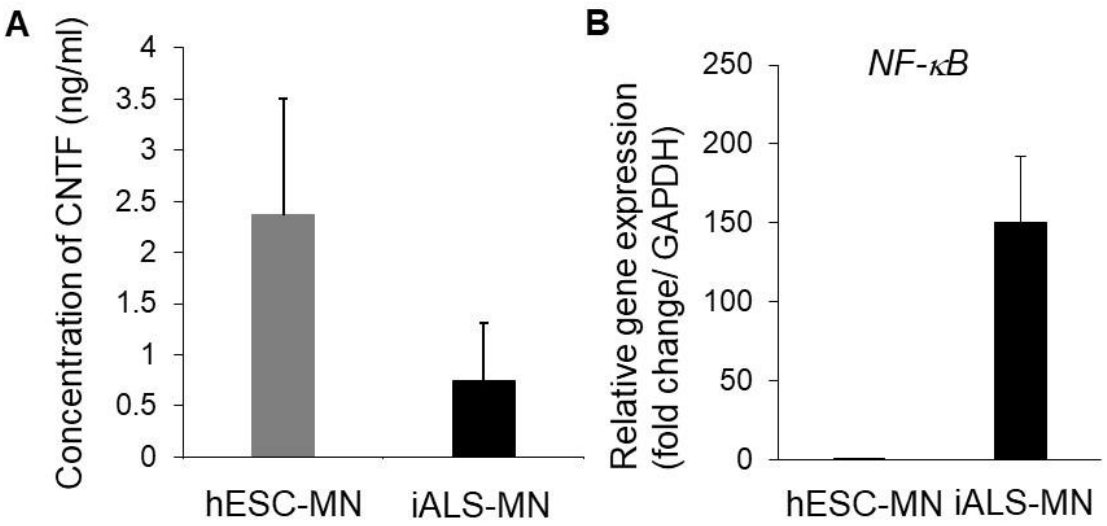

Fig. S9. Significant loss of CNTF secretion in iALS-MN accelerated apoptosis of muscle cells. (A) Concentration of CNTF decreased in iALS-MN compared to hESC-MN after co-culture with muscle cells in a microfluidic device. (n = 3) (B) Relative expression of NF-*k*B in MN after co-culture with muscle tissues in microfluidic devices. The expression in iALS-MN significantly increased due to the OPTN mutation via dysfunction of NF-*k*B suppressive activity. (n = 5).

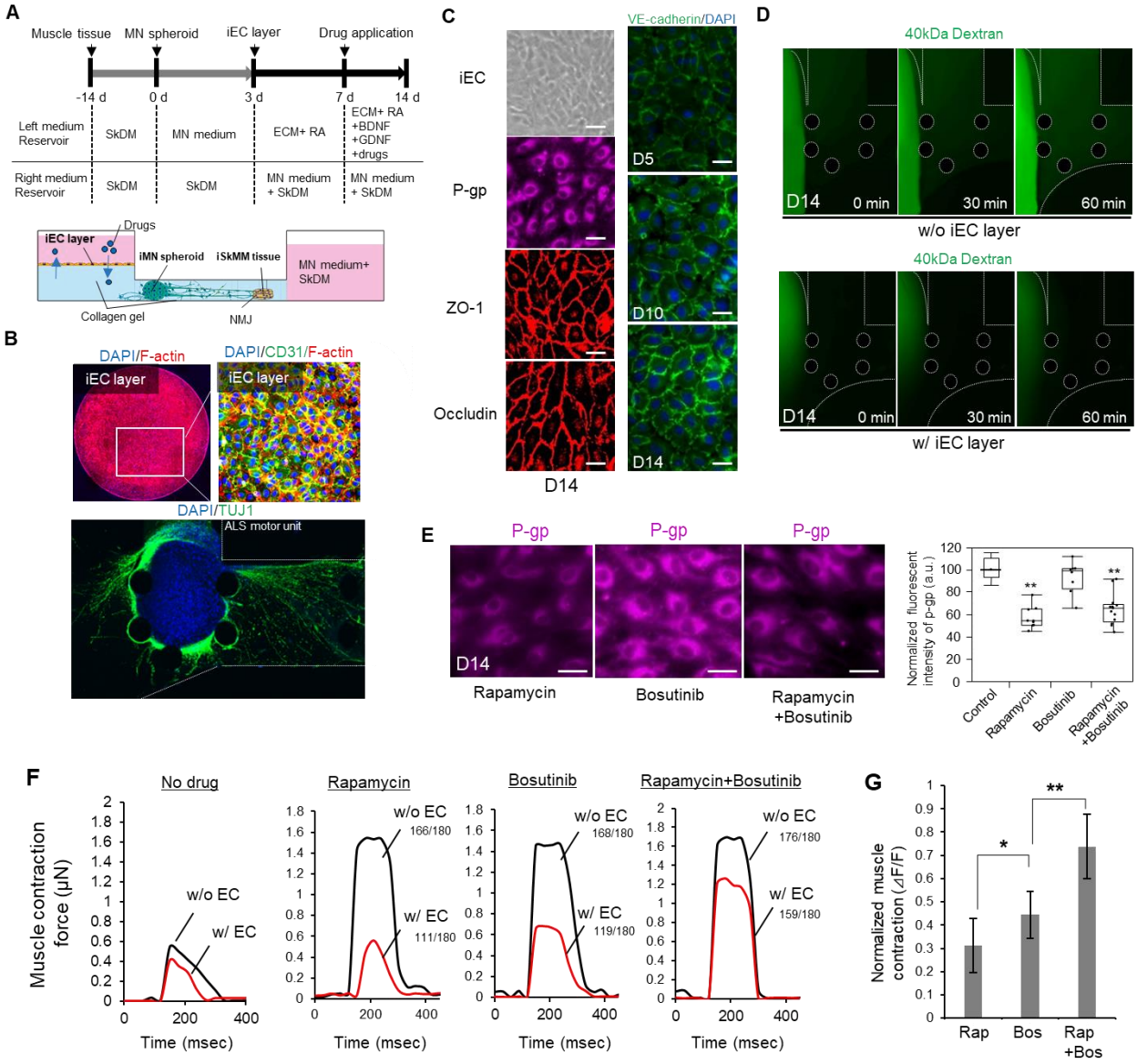

Fig. S10. Drug application through the iEC barrier. (A) Culture scheme of iEC layer, iALS-MN spheroid, and iPSC-derived skeletal muscle fiber bundle. (B) Formation of iEC layer on collagen gel in left medium reservoir and immunostaining of F-actin and CD31 on D14. Scale bars, 100 μm. (C) Immunostaining of P-glycoprotein (P-gp), ZO-1, and occludin to characterize the phenotype of iEC. VE-cadherin expression of iEC layer at D5, D10, and D14. Scale bars, 20 μm. (D) The permeability through iEC layer after D14 of culture. FITC-tagged 40 kDa dextran was applied to left medium reservoir. iEC layer prevents diffusion of dextran. (E) Immunostaining of P-gp at three conditions. Rapamycin treatment significantly decreases P-gp expression. Scale bars, 20 μm. (F) The comparison of muscle contraction with and without iEC layer in the presence of no drug, rapamycin, and bosutinib, and co-treatment with both. (G) Normalized muscle contraction by treatment of drugs via iEC layer copared to without iEC layer. (n = 4). *, P<0.05. **, P<0.01. one-way ANOVA. The bars of each column indicate range.

Table S1. Primer sequences for real-time RT-PCR.

Target gene	Forward primer sequence(5'-3')	Reverse primer sequence(5'-3')
GAPDH (human)	TGT GGG CAT CAA TGG ATT TGG	ACA CCA TGT ATT CCG GGT CAA T
Myogenin	GGG GAA AAC TAC CTG CCT GTC	AGG CGC TCG ATG TAC TGG AT
MyoD	CCA CCG GAA GTT GCA GAC A	GGA ACT CGC AGA ACA GGC A
FHL1	TGC TGC CTG AAA TGC TTT GAC	GCCAGAAGCGGTTCTTATAGTG
Nestin	GTC TCA GGA CAG TGC TGA GCC TTC	TCC CCT GAG GAC CAG GAG TCT C
E-cadherin	AAA GGC CCA TTT CCT AAA AAC CT	TGC GTT CTC TAT CCA GAG GCT
SOX1	GCG GAA AGC GTT TTC TTG	TAA TCT GAC TTC TCC TCC C
PAX6	AGT GCC CGT CCA TCT TTG C	CGC TTG GTA TGT TAT CGT TGG T
Oligo2	CCA GAG CCC GAT GAC CTT TTT	CAC TGC CTC CTA GCT TGT CC
NGN2	AGG AAG AGG ACG TGT TAG TGC	GCA ATC GTG TAC CAG ACC CAG
Neuro D1	GGA TGA CGA TCA AAA GCC CAA	GCG TCT TAG AAT AGC AAG GCA
HB9	CTT TTT GCT GCG TTT CCA TT	GCA CCA GTT CAA GCT CAA CA
Islet1	GCG GAG TGT AAT CAG TAT TTG GA	GCA TTT GAT CCC GTA CAA CCT
ChAT	GGA GCC TGA GCA CGT CAT C	CAA CTG AGT GAA CAG ATC CCC
Lim3	GGA GAG CGT TTA CTG CAA GGA	TTG GCG GTT TCG TAG TCC G
NeuN	GAC GCA ATG GTT CAG CCT TTT	GCG TAC TTC CGT AGA GTG TCA G
Chox10	TCA TGG CGG AGT ATG GGC T	TCC AGC GAC TTT TTG TGC ATC
En1	GAG CGC AGG GCA CCA AAT A	CGA GTC AGT TTT GAC CAC GG
Evx1	GAC CAG ATG CGT CGT TAC CG	GTG GTT TCC GGC AGG TTT AG
SMI-32	GCA GTC CGA GGA GTG GTT C	CGC ATA GCG TCT GTG TTC A
Synapsin I	AGT TCT TCG GAA TGG GGT GAA	CAA ACT GCG GTA GTC TCC GTT
VAChT	CTG CTA GTG AAC CCC TTG AGC	CAG GAC TGT AGA GGC GAA CAT
p75	CCT ACG GCT ACT ACC AGG ATG	CAC ACG GTG TTC TGC TTG T
GFAP	CTG CGG CTC GAT CAA CTC A	TCC AGC GAC TCA ATC TTC CTC
OSP	CGG TGT GGC TAA GTA CAG GC	CGC AGT GTA GTA GAA ACG GTT TT
SOX10	CCT CAC AGA TCG CCT ACA CC	CAT ATA GGA GAA GGC CGA GTA GA
HIF-1a	CAG CTT CCT TCG GAC ACA TAA G	CCA CAG CAA TGA AAC CCT CCA
Ki67	ACG CCT GGT TAC TAT CAA AA GG	CAG ACC CAT TTA CTT GTG TTG GA
NEFL	GAG TGG CTT TCG GCT TGC T	CAC ATT GCC GTA GAT CCT GAA CT
NEFM	AAG GCA GTG GGA GGG AAG AG	TTC ATC TGC TGG GCT CAA GTC
TARDBP	GCG CTG TAC AGA GGA CAT GA	AGT TCA TCC CAC CAC CCA TA
ATG5	AAA GAT GTG CTT CGA GAT GTG T	CAC TTT GTC AGT TAC CAA CGT CA
ATG7	ATG ATC CCT GTA ACT TAG CCC A	CAC GGA AGC AAA CAA CTT CAA C
ATG16L2	TGG ACA AGT TCT CAA AGA AGC TG	CCT CAG TGC GAC CAG TGA T
BECN1	CCA TGC AGG TGA GCT TCG T	GAA TCT GCG AGA GAC ACC ATC
ULK1	AGC ACG ATT TGG AGG TCG C	GCC ACG ATG TTT TCA TGT TTC A
ULK2	TGG AGA CCT CGC AGA TTA TTT GC	CTG TGC AGG ATT CGC ATG G
NF-kB1	AAC AGA GAG GAT TTC GTT TCC G	TTT GAC CTG AGG GTA AGA CTT CT
LC3	AAC ATG AGC GAG TTG GTC AAG	GCT CGT AGA TGT CCG CGA T
MYH1	CCC TAC AAG TGG TTG CCA GTG	CTT CCC TGC GCC AGA TTC TC
MYH2	CTG AGG GAG GAG CGA CTC T	CTC GGG CTT ATA CAC AGG CA
MYL1	TTG GGC GAG TGA ACG TGA AAA	CCG AAC GTA ATC AGC CTT CAG
Caspase-3	GAA ATT GTG GAA TTG ATG CGT GA	CTA CAA CGA TCC CCT CTG AAA AA
Caspase-7	CGG TCC TCG TTT GTA CCG TC	CGC CCA TAC CTG TCA CTT TAT CA
Caspase-8	GTT GTG TGG GGT AAT GAC AAT CT	TCA AAG GTC GTG GTC AAA GCC
Caspase-9	CTC AGA CCA GAG ATT CGC AAA C	GCA TTT CCC CTC AAA CTC TCA A
Caspase-10	TAG GAT TGG TCC CCA ACA AGA	GAG AAA CCC TTT GTC GGG TGG

Table S2. SNP mutation (whole-exome sequencing), ALS pathogenesis related.

Category	Gene	SNP mutation, insertion, and deletion (Red: missense, frameshift)
ALS pathogenesis associated	SOD1	No variants found
	C9orf72	Chr9: 27558547 C/T HET, chr9: 27561466 -/TGT insertion HOM (rs3063748), chr9: 27567145 C/T HET (rs10757668, UTR)
	TARDBP	Chr1:11082538 A/G HET (rs4884357, G298S), chr1: 11082107 -/T insertion HET (rs202106921)
	TBK1	Chr12: 64875787 A/T HET (rs7486100, intron)
	NEK1	Chr4: 170315496 C/T HOM (rs4692721, UTR), chr4: 170482883 A/G HOM (rs560644008, intron) Chr4: 170506703 A/G HOM (rs55679731, intron)
	OPTIN	Chr10: 13150991 -/CACA insertion HET (rs111744244), chr10: 13151224 G/A HET (rs2234968, T34T) chr10: 13151245 G/A HET (rs11591687, L41L), chr10: 13158262 C/T HOM (rs2244380), chr10: 13166076 A/G HOM (rs523747, E322K), chr10: 13174098 A/G HET (rs267606929, E478G)
	SPG11	Chr15: 44918690 C/T HET (rs78183930, A695T), chr15: 44943757 A/G HOM (rs3759871, F463S) chr15: 44944037 C/T HET (rs77697105, E370K)
	VCP	Chr9: 35056961 C/A HET (rs1053318, UTR), chr9: 35062973 C/T HOM (rs514492, intron)
	ATXN2	Chr12: 1120336754-756 -/GCT deletion (rs10560189), chr12: 112036797 C/T HOM (rs4098854, Q174Q)
	ANG	Chr14: 21162053 T/G HET (rs11701, G110G)
	CHCHD10	Chr22: 24108412 G/A HOM (rs9153, Y104Y), chr24109744 T/G HOM (rs179468, P16P)
	SIGMAR1	Chr9: 34635598 T/C HOM (rs4879809, UTR)
	FIG4	Chr6: 110106234 A/G HOM (rs10499054, intron), chr6: 110146588 C/T HOM (rs1127775, UTR)
	SS18L1	No variants found
	GRN	No variants found
	SETX	Chr9: 135152544 A/- deletion HET (rs34769225), chr9: 135202829 T/C HOM (rs543573, I1386V) chr9: 135203231 C/T HOM (rs1183768, G1252R), chr9: 135203409 A/C HOM (rs1185193, D1192E) chr9: 135206460 A/G HOM (rs9411449, Y359Y)
	SQSTM1	No variants found
	TAF15	No variants found
	FUS	Chr16: 31191482 A/G HOM (rs929867, UTR), chr16: 31195279 C/T HOM (rs1052352, Y97Y) chr16: 31203320 C/T HET (rs192705444), chr16:31204235 T/C HOM (rs11860134, UTR)
	ALS2	Chr2: 202575821 G/A HET (rs3219168, L1339L), chr2: 202580514 C/T HET (rs34946105, A1295A), chr2: 202625615 C/T HET (rs3219156, V368M)
	VAPB	Chr20: 57020741-758 TGTGTGTGTGTGTGTGTG/- deletion HET (rs138225455) chr20: 57022713-720 TGTGTGCA deletion HOM (rs112902943), chr20: 57023343 C/T HET (rs76295834, UTR), chr20: 57023737 G/A HET (rs79623348, UTR) chr20: 57024159 C/T HET (rs74748993, UTR), chr20: 57024541 T/C HET (rs6015274, UTR) chr20: 57024589 C/T HET (rs6015275, UTR), chr20: 57025379 C/T HET (rs147304840, UTR) chr20: 57025404-410 TCTG/- deletion HET (rs143261907)
	NEFH	Chr22: 29885567 A/C HET (rs75808076, A646A), chr22: 29885594 A/T HET (rs79235463) chr22: 29885861 T/C HOM (rs165923, A744A) chr22: 29886413 C/G HOM (rs165625, V928V), chr22: 29886893 G/T HOM (rs1061373, UTR)
	MATR3	Chr5: 138609609 C/G HOM (rs11242456, UTR), chr5: 138643062 T/A HOM (rs12153162, intron) chr5: 138665756 G/A HET (rs7305, UTR), chr5: 138666372 T/G HOM (rs10515507, UTR) chr5: 138667325 A/G HET (rs886060006, UTR)
	PFN1	No variants found
	SPAST	Chr2: 32340779 G/A HET (rs145264166, P293P), chr2: 32379449 A/C HET (rs144594804, N579H)
	TUBA4A	No variants found
	ELP3	No variants found
	DAO	No variants found

Table S2. SNP mutation (whole-exome sequencing), ALS pathogenesis related, continued

Category	Gene	SNP mutation, insertion, and deletion
ALS pathogenesis associated	ANO9	Chr11: 428385 A/G HOM (rs10794323), chr11: 428489 T/C HOM (rs10794324) chr11: 433387 A/G HOM, chr11: 433867 G/A HET (rs12575508)
	DCTN1	No variants found
	UBQLN2	No variants found
	GPR158	Chr10: 25701341 C/G HOM (rs2480345)
	GREB1L	Chr18: 19079853 A/G HOM (rs4800747), chr19100759 -/TCT insertion HOM (rs34960489)
	IMPG2	Chr3: 100949842 G/A HOM (rs348867, L1127L)
	ERBB4	Chr2: 212251864 T/C HOM (rs3748962)
	APEX1	Chr14: 20925154 T/G HET (rs1130409, D148E)
	CHMP2B	No variants found
	NEFL	Chr8: 24810088 T/A HOM (rs1059111, UTR), chr8: 24811071 G/- deletion HOM (rs397788090, frameshift)
	NEFM	Chr8: 24774683 C/A HOM (rs196864, P439T)
	PON1	Chr7: 94946084 A/T HET (rs854560, L55M)
	PON2	No variants found
	PON3	No variants found
	PRPH	No variants found
	SMN1	No variants found
	SMN2	No variants found
	VEGF	No variants found

Table S3. SNP mutation (whole-exome sequencing), ATG family.

Category	Gene	SNP mutation, insertion, and deletion
ATG family	ATG1	No variants found
	ATG2A	Chr11: 64677293 G/C HOM (rs656195), chr11: 64680819 G/A HET
	ATG2B	Chr14: 96771959 A/G HOM (rs2289622), chr14 96781912 T/C HOM (rs9323945), chr14: 96797724 G/A HOM (rs1822372)
	ATG3	Chr3: 112253059 -/A insertion HOM (rs35560667), chr3: 112280706 C/G HOM (rs2399431)
	ATG4A	No variants found
	ATG4B	Chr2: 242610738 T/C HOM, chr2: 242610773 T/A HOM, chr2: 242612064 -/G insertion HOM (rs34358233)
	ATG4C	No variants found
	ATG4D	Chr19: 10659659 C/T HET
	ATG5	No variants found
	ATG7	Chr3: 11596897 A.G HOM
	ATG9A	Chr2: 220084902 G/A HOM (rs3755048), chr2: 220085845 A/G HOM (rs2276633)
	ATG9B	Chr7: 150713827 G/A HET (rs3800789), chr7: 150713902 -/C insertion (rs11393607)
	ATG10	No variants found
	ATG12	Chr5: 115176589 A/G HOM (rs26536),
	ATG13	Chr11: 46694313 TC/- deletion
	ATG14	Chr14: 55864130 A/G HET (rs8003279)
	ATG16L2	Chr11: 72532708 C/T HOM (rs11235603), chr11: 72540633 -/TCTA insertion HET(rs144487404)

Table S4. SNP mutation (whole-exome sequencing), autophagy related.

Category	Gene	SNP mutation, insertion, and deletion
Autophagy related	BCL2	Chr18: 60795541 C/T HET, Chr18:60985879 T/C HET, chr18:60986549 C/G HOM(rs1473418),
	BCL2L1	No variants found
	BECN1	Chr17: 40963597 C/T HET(rs117018379),
	CASP3	No variants found
	CASP8	Chr2: 202122995 A/G HOM, chr2: 2021151439 G/C HOM,
	CLN3	No variants found
	CXCR4	Chr2: 136873549 A/T HET (rs2680880),
	FADD	Chr11: 70049523 A/G HOM (rs1131677)
	FAS	Chr10: 90771829 T/C HET (rs2234978), chr10: 90775291 C/T HET
	HTT	Chr4: 3076603-06 CAGCAG/CAGCAGCAG (rs374076986), chr4: 3219613 A/C HOM
	IFNG	No variants found
	IGF1	No variants found
	TNF	No variants found
	TNFSF10	No variants found
	TP53	Chr17: 7578645 C/T HOM, chr17:7578712-8714 TTT/- deletion (rs141204613)
	ULK1	Chr12: 132396603 C/T HOM (rs11616018), chr12: 132401050 C/T HET (rs61731334), chr12: 132402020 T/C HOM (rs4964918), chr12: 132403161 A/G HOM (rs11609348). Chr12: 132406275 A/C HOM (rs7311029)
	ULK2	Chr17: 19702892 -/AA insertion HET (rs34321770), chr17: 19713740 C/T HOM (rs150122)

Movie S1. Image stacks of muscle fiber bundle stained with α-actinin (green) and DAPI (blue).

Movie S2. 3D construction of muscle fiber bundle based on iPSC-derived skeletal muscle cells.

Movie S3. Representative movie of muscle contraction after stimulation with glutamic acid on day 14.

Movie S4. Muscle contraction of the ALS motor unit after 1-Hz optical stimulation without drug.

Movie S5. Muscle contraction of the ALS motor unit after 1-Hz optical stimulation with rapamycin.

Movie S6. Muscle contraction of the ALS motor unit after 1-Hz optical stimulation with rapamycin and bosutinib.